Effect of Silica-Based Nanofillers on the Properties of a Low-Density Polyethylene/Ethylene Vinyl Acetate Copolymer Based Thermoplastic Elastomer

S. Hui, T. K. Chaki, S. Chattopadhyay

Rubber Technology Centre, Indian Institute of Technology, Kharagpur, India 721302

Received 14 November 2007; accepted 10 April 2008
DOI 10.1002/app.28537
Published online 10 July 2008 in Wiley InterScience (www.interscience.wiley.com).

ABSTRACT: The effect of pristine silica nanoparticles on a model low-density polyethylene (LDPE)–ethylene vinyl acetate copolymer (EVA) thermoplastic elastomer blend system is explored in this article. Pristine silica nanoparticles were melt-blended with the LDPE–EVA system at 1.5, 3, and 5 wt % loadings through the variation of the sequence of addition. In one of the compositions, coupling agent bis[3-(triethoxysilyl)propyl] tetrasulfide (Si-69) was used to improve the interaction of hydrophilic silica fillers with the polymer matrix. The blends were compression-molded, and their mechanical, dynamic mechanical, and thermal properties, X-ray diffraction patterns, and morphology were evaluated. The properties of the blends were found to be strong functions of the sequence of addition of nanofillers during their preparation. With Si-69 as a coupling agent, the dynamic storage modulus of nanosilica-based composites was found to increase up to 35%. An appreciable improvement in the tension set properties of the thermoplastic elastomer nanocomposites was observed in all the nanosilica-based films. Morphological studies and dynamic properties clearly indicated that the differential properties of these blend systems primarily stemmed from the extent of dispersion and alternation of crystalline morphology, which in turn was a strong function of preferential incorporation in the LDPE or EVA matrix and the agglomeration tendency of the nanofillers. © 2008 Wiley Periodicals, Inc. J Appl Polym Sci 110: 825–836, 2008

Key words: blends; crystallization; dispersions; morphology; nanocomposites

INTRODUCTION

In recent years, novel materials have been continuously produced for specific requirements because of the very fast growth and development of industrial activities around the world. Polymer blending has been proven to be an economical and promising route for innovating and developing new polymeric materials. To widen the diversity of available polymers, another well-known approach is to modify their technical properties by the addition of fillers. Fillers are solid additives that differ from polymers in both their chemical and physical composition and structure. The vast number of fillers includes silica,[1–3] glass fibers,[3,4] carbon black,[5,6] talc,[7] clay,[8,9] titanates,[10] and calcium carbonate,[11] to mention a few. These have been used for multicomponent systems to achieve a broader assortment of properties. Currently, nanostructured fillers have become the main focus of attraction in polymer industries. There has been renewed interest in the influence of nanoparticles on the behavior of polymer systems (homopolymers, blends, or block copolymers).[12–30] This interest originates from the fact that the addition of a small amount of nanoparticles can dramatically change a myriad of properties of polymers, such as the modulus of elasticity, gas-barrier property, electrical conductivity, magnetic susceptibility, hardness, abrasion resistance, static and dynamic mechanical properties, scratch resistance, adhesive strength, and ultraviolet protection, and they can be widely used in applications such as coatings, rubbers, plastics, sealants, and fibers.[31–36]

Recently, one area that has come under intense inspection is the role of nanoparticles as potential compatibilizers for mixtures of immiscible polymers. Recent simulations by Ginzberg and coworkers,[12–14] Zhu and Ma,[15] and Laradji and McNevin[16,17] revealed that nanoparticles can be distributed between two polymers even when the particles themselves have a strong preference toward one of the two polymeric components. Experimentally, Lipatov and coworkers[19–21] studied the influence of silica nanoparticles on the cloud point of a poly(vinyl alcohol)/poly(methyl methacrylate) mixture. Lipatov et al.[21] postulated that nanoparticles, under some conditions, play the role of a compatibilizer in a

Correspondence to: S. Chattopadhyay (santanuchat71@yahoo.com).

Contract grant sponsor: Department of Science and Technology (New Delhi, India); contract grant number: SR/FTP/ETA-15/2005.

Contract grant sponsor: Council of Scientific and Industrial Research (New Delhi, India).

© 2008 Wiley Periodicals, Inc.

binary polymer blend system, and they formulated a semiphenomenological theory to explain this. However, this theory does not explicitly take the particle size or geometry or interfacial behavior into account and, in general, has a somewhat narrow degree of predictability. There have been other experimental studies concerning the distribution of nanoparticles (e.g., carbon) in polymer blends,[22–24] but no theoretical analysis of the influence of particles on the phase behavior of systems has been discussed. The morphology plays a critical and influential role in the performance of multiphase blends. The blend morphology initially depends on the way in which the blend components interact when the individual blend components are brought into physical contact, and it ends when the structure becomes frozen in only at the beginning of the development of the microstructure. In immiscible multiphase polymer blends, one component forms the discrete phase, and it is dispersed in the host component, which acts as a continuous phase. Generally, new properties are achieved through this dispersed phase, which can exist in the form of droplets, fibrils, lamellae, or even cocontinuous structures after blending.[37–41] The state of distribution and dispersion of filler particles between the two phases, the extent of interaction of the filler surface with either of the polymeric phases, and the resultant final phase morphology are believed to be the most important factors affecting the overall properties of the final blends. However, there are many factors that control the filler distribution and dispersion. These include the affinity of the filler toward the polymeric phases, the viscosity ratio of the polymers, and the feeding routes.[42] It has also been reported that nanofillers significantly alter the crystalline structure of semicrystalline polymers. Therefore, the technical properties of the blends are modified to a marked extent. Thus, in the case of polymer blend nanocomposites, the microscale morphology as well as the nanoscale filler distribution and crystalline structure could dictate the resultant properties of the composites.[43–46]

A thermoplastic elastomer (TPE) blend system derived from low-density polyethylene (LDPE) and ethylene vinyl acetate copolymer (EVA) has been chosen for this study. In TPEs, the functional properties of conventional crosslinked thermoset elastomers and the favorable processing characteristics of thermoplastics are brought together.

However, if rubber and plastic are blended to produce a TPE, their technical properties are inferior because of the presence of a weak rubbery phase and an interface dispersed in a continuous plastic matrix. This limitation can be circumvented by preferential reinforcement of the rubber phase and the interface with the plastic matrix by fillers and/or the addition of crosslinks in the rubbery phase via dynamic vulcanization without the processing characteristics being sacrificed. Goettler et al.[47] addressed the partitioning of clay reinforcement in two-phase heterogeneous polymer blends including thermoplastic vulcanized (TPV) systems. The microstructure–property correlation in dynamically vulcanized nanocomposite TPEs based on polypropylene/ethylene–propylene–diene monomer was studied by Naderi et al.[48] However, a TPV system is not the subject matter of this work. Pukanszky[49] proposed that the dimensions of the interface and strength of the interaction significantly influence the ultimate tensile properties of composites. Different authors have investigated the properties and various aspects of filled polymer blend systems.[50–52] The sequence of addition of the individual polymers and fillers also plays an important role in determining the properties of polymer blends. The influence of the blending sequence on the technical properties and energy consumption in polymer blending was studied by Mukhopadhyay et al.[53] Conductive polypropylene/polyamide blends with a low carbon black loading were studied by Tchoudakov et al.[54] The effects of the blending sequence and interfacial agent on the morphology and mechanical properties of injection-molded polycarbonate/polypropylene blends were studied by Torres et al.[55] The effect of the blending sequence on the microstructure of nylon 66/organoclay/styrene-ethylene/butylene-styrene (SEBS-*g*-MA) based ternary nanocomposites was studied by Dasari et al.[56] Dasari et al. also studied the microscale and nanoscale deformation behavior of nylon 66/organoclay/SEBS-*g*-MA ternary nanocomposites.[57] Selective distributions of fillers as well as their state of dispersion in a particular phase are strongly dependent on their interaction with individual polymers and the extent of shear stress that is being applied to overcome a high degree of viscosity barrier during their preparation. However, to the best of our knowledge, no references are available in the literature dealing with the selective distribution and dispersion of nanosilica fillers in TPE blends.

In this work, the effect of nanosilica on an LDPE/EVA-based TPE blend has been investigated. It is well-known that silica as a filler exhibits a filler networking or aggregation tendency because of its poor compatibility with hydrocarbon rubber, its polar nature, and its ability to form hydrogen bonds. To improve the adhesion between the polymeric matrix and inorganic particles, coupling agents are generally employed to modify the surfaces of inorganic particles. Silane coupling agents are often used to treat the silica filler because of their unique bifunctional structure along with one end capable of reacting with the silanol groups on the silica surface, whereas the other end is compatible with the

TABLE I
Sample Designations

Sample code	LDPE (wt %)	EVA (wt %)	SiO_2 (wt %)	Sequence of silica addition
EL 6/4	40	60	0	—
ELS 6/4/1.5	40	60	1.5	3
ELS 6/4/3-1	40	60	3	1
ELS 6/4/3-2	40	60	3	2
ELS 6/4/3-3	40	60	3	3
ELS 6/4/3-3/Si-69	40	60	3 phr + 10% Si-69	3
ELS 6/4/5	40	60	5	3
L 100	100	0	0	—
E 100	0	100	0	—

E, EVA; L, LDPE; S, silica.

polymer matrix. The reaction of bis[3-(triethoxysilyl)-propyl] tetrasulfide (Si-69) with silica during mixing is always more economical than modifying the fillers separately before mixing. The distribution of the silica between the two polymeric phases under melt-mixing conditions and its effect on the interface have been closely followed by means of scanning electron microscopy (SEM) and atomic force microscopy (AFM). The effects of changes in the microscale and nanoscale morphology and crystallinity [evaluated by differential scanning calorimetry (DSC) and X-ray diffraction (XRD)] and variations in the silica loading, sequence of addition, and use of a coupling agent on the mechanical and dynamic mechanical properties have been investigated in this work. A system consisting of an organic polymer and inorganic particles can be considered a unique model system for studying the structure and dynamics of polymers in confined environments that can bring new breadth to the science and technology of next-generation TPE-based materials.

EXPERIMENTAL

Materials

The plastic used for this work was LDPE (Indothene MA 400) supplied by IPCL (Vadodera, India; density = 0.918 g/cm^3, melt index = 3°/min). The elastomer was EVA-40 [melt flow index (per ASTM D 1238 at 190°C with a 2.16-kg load) = 3], which was kindly provided by Nicco Corp., Ltd. (Shyamnagar, India). Silicon dioxide nanopowder and Si-69 were procured from Aldrich Chemical Co., Ltd. (Milwaukee, WI).

Sample preparation

Melt blending was carried out with EVA and LDPE with various loadings of silicon dioxide powder (1.5, 3, and 5 wt %) in a Brabender PLE-330 plasticorder (Duisburg, Germany) at 130°C and a rotor speed of 80 rpm by the variation of three different sequences. In sequence 1, LDPE was first allowed to melt for 4 min; it was followed by EVA, and afterwards, the silica particles were added. The total mixing time was 10 min. Then, they were remixed for another 2 min. In sequence 2, first LDPE was allowed to melt for 4 min, and it was followed by silica for 4 min at 130°C. They were remixed for 2 min. Then, first LDPE and the particles were mixed at 130°C; this was followed by EVA, and the total mixing time was 6 min. They were remixed for 2 min. In sequence 3, first EVA was allowed to melt for 4 min, and it was followed by silica particles for 4 min at 110°C. Then, LDPE was allowed to melt for 4 min at 130°C, and this was followed by an EVA–particle mixture (which was previously made at 110°C) for 2 min at 130°C. The mixes so obtained were sheeted out through an open mill set with a 2-mm nip gap. Then, they were remixed in the Brabender plasticorder for another 2 min at 130°C.

The sheets were compression-molded between two Teflon sheets for 3 min at 150°C with a preheating time of 1 min and a pressure of 5 tons in an electrically heated hydraulic press to obtain films 0.03–0.04 cm thick. The moldings were cooled under compression to maintain the overall dimensional stability. The details of the samples and their appropriate designations are given in Table I.

Microscopy studies

SEM

To study the developed morphology of the polymer blends, SEM examination was performed on gold-coated surfaces of the sample films (etched with methyl ethyl ketone) with a JSM 5800 microscope (JEOL, Tokyo, Japan). The accelerating voltage of the beam was 15 kV. Characteristic X-rays of silicon were emitted because of electron bombardment of the nanocomposites. The X-ray silicon dot maps of the samples were recorded with an Oxford Isis-300 energy-dispersive X-ray (EDX) microanalytical

system (Oxford Instruments, Oxford, United Kingdom) attached to the JEOL JSM 5800 scanning electron microscope. EDX analysis dot mapping was performed on smooth sample films sputter-coated with a very thin gold coating, and the dot maps presented here correspond to sample topography at a 500× magnification. The white points in the figures denote Si–X-ray signals.

AFM

AFM images of the sample films were recorded in air at 25°C with a Nanoscope III Dimension Zero atomic force microscope made by Digital Instruments, Inc. (Santa Barbara, CA). The experiments were carried out on cryotomed samples in the tapping mode with microfabricated cantilevers. The nanoprobe tip was made of silicon nitride, and it was square-pyramidal in shape with base dimensions of approximately 4 μm × 4 μm. The characteristics of the silicon nitride probe were a spring constant of 0.58 N/m, a normal tip radius of curvature of 20 nm, a cantilever length of 100 μm, a V-shaped cantilever configuration, a reflective coating of gold, and a sidewall angle of 35° on all four sides.

DSC studies

DSC analysis was performed on a TA Instrument DSC Q100 from −130 to 150°C at 10°C/min in a nitrogen atmosphere. The peak minima from the melting thermogram were considered the melting points. To compare the crystallinity, the areas under the melting peak were used, and these were computed with Q series software.

XRD

The XRD patterns of the samples were recorded with a Philips PW-1710 X-ray diffractometer (Eindhoven, The Netherlands) with crystal monochromated Co Kα radiation in the angular range of 10–35° (2θ) with a 40-kV operating voltage and a 20-mA current. The areas under the crystalline and amorphous portions were determined in arbitrary units, and the percentage of crystallinity (κ_c) was measured with the following relation:

$$\chi_c = \frac{I_c}{I_c + I_a} \times 100 \quad (1)$$

where I_a and I_c are the integrated intensities corresponding to the amorphous and crystalline phases, respectively. The 2θ values could be reproduced within a variation of ±0.02°.

The crystalline size (P), interchain distance (r), and interplanar distance (d) were calculated as follows:

$$P = \frac{k.\lambda}{\beta \cos\theta} \quad (2)$$

$$r = \frac{5.\lambda}{8 \sin\theta} \quad (3)$$

$$d = \frac{\lambda}{2 \sin\theta} \quad (4)$$

where β is the half-height width (rad) of the crystalline peak, λ is the wavelength of the X-ray radiation (1.79 Å), and k is Scherrer's constant[58] (taken to be 0.9). The results reported here were based on averages of three experiments.

Mechanical properties

The specimens for the measurement of the mechanical properties were punched out from the molded films with ASTM Die-C. The measurement was carried out in a Hioks–Hounsfield universal testing machine (Test Equipment, Ltd., Surrey, England) at a crosshead speed of 100 mm/min at 25°C. The averages of three tests are reported here. The force–elongation curve was plotted with Lab Tensile software, from which the tensile strength and elongation percentage were calculated. The tension set properties were measured with a similar tensile sample by elongation up to 100% elongation for 10 min, and the percentage set was measured after equilibration for another 10 min.

Dynamic mechanical analysis (DMA)

DMA was carried out with a DMA 2820 (TA Instrument) in the dual-cantilever mode. The experiments were carried out at a frequency of 1.0 Hz. The measurements were taken at a heating rate of 2°C/min and a double-strain amplitude of 100 μm. A temperature scan was performed between −60 and 80°C. The storage modulus and loss tangent (tan δ) values were measured for all samples under identical conditions.

RESULTS AND DISCUSSION

Microscopy studies

In Figure 1(a–g), SEM photomicrographs of unfilled and filled polymers are displayed. The black domains indicate the positions of the extracted EVA phase. In control sample EL 6/4 with 40 wt % LDPE, LDPE is found as the continuous matrix. The molten polymeric materials during melt mixing experience high shearing actions. The induced shearing force deforms the dispersed molten polymer into elongated, rodlike particles, which progressively

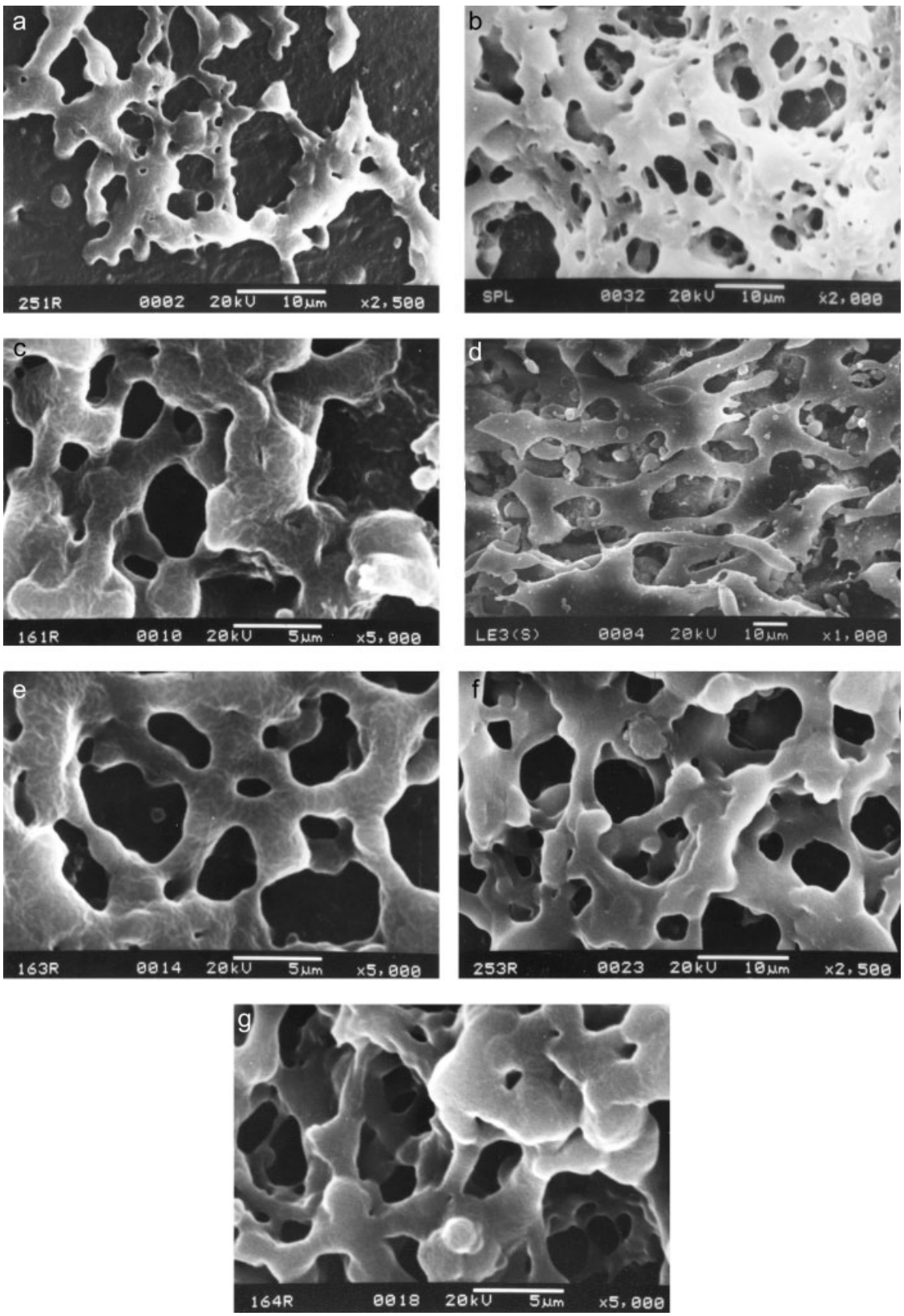

Figure 1 SEM photomicrographs of methyl ethyl ketone etched samples of 60 : 40 EVA–LDPE blends with various loadings of silica particles: (a) EL 6/4, (b) ELS 6/4/1.5, (c) ELS 6/4/3-1, (d) ELS 6/4/3-2, (e) ELS 6/4/3-3, (f) ELS 6/4/3-3/Si-69, and (g) ELS 6/4/5.

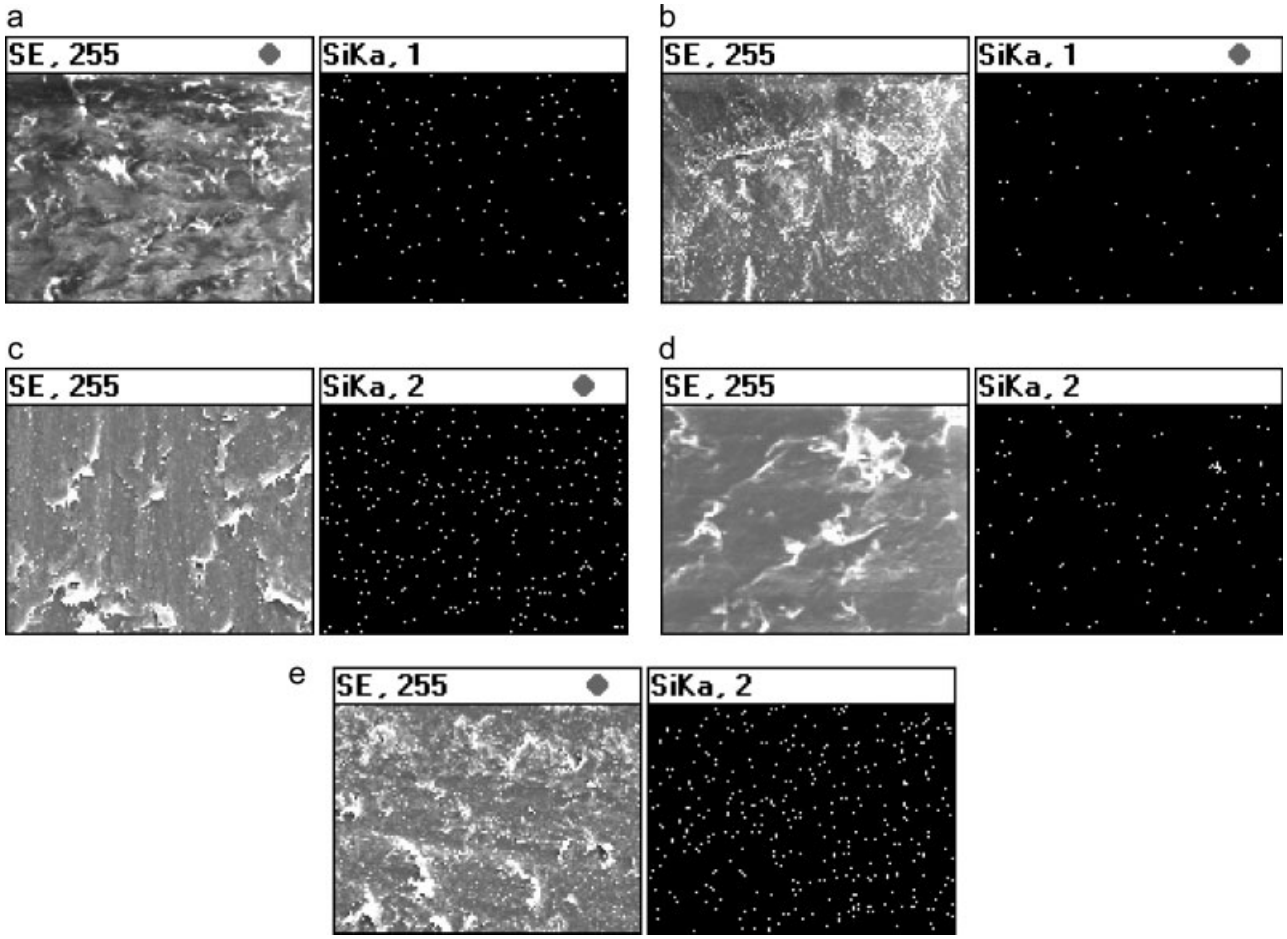

Figure 2 X-ray silicon dot mapping of 60 : 40 EVA–LDPE blends with various loadings of silica: (a) ELS 6/4/3-1, (b) ELS 6/4/3-2, (c) ELS 6/4/3-3, (d) ELS 6/4/3-3/Si-69, and (e) ELS 6/4/5. In each set, the left image is a 500× magnified image of the sample surface, and the right image is the corresponding dot mapping. [Color figure can be viewed in the online issue, which is available at www.interscience.wiley.com.]

constrict until rupture. During mixing and molding when the polymers come out of the shearing zone, they may fully or partly relax to regain their original spherical, elliptical, or elongated elliptical shapes and may remain isolated from one another. However, there is also a tendency for recombination, leading to intricate shapes.

In control blends, the two components of the blends (LDPE and EVA 40) have different polarities and melt viscosities. Thus, an immiscible blend morphology is expected. Because of the high melt flow index or low melt viscosity of LDPE, the blends preferentially have LDPE as a continuous matrix, even with a higher proportion of EVA, although they partly retain the feature of a cocontinuous morphology as well.

In SEM photomicrographs of filled polymer matrices with different filler loadings, the presence of silica particles on the LDPE matrix is not clearly visible, except in sequence 2. In sequence 3, the average size of the EVA phase becomes larger upon the silica loading increasing. This may be due to the decrease in the flowability of EVA upon the nanosilica loading. Also, in comparison with the blends prepared by sequence 3, the average size of the EVA phase is smaller in the case of the blend prepared via sequence 1. Sequence 2 exhibits a cocontinuous morphology only. In this case, silica aggregates appear clearly on LDPE phases. Upon the addition of a silane coupling agent, the average size-scale distribution of EVA domains becomes narrower, although the overall domain size increases.

From X-ray dot mapping (EDX; Fig. 2), it can be observed that the aggregation tendency of the nanosilica is more in sequence 3 than in sequence 1, whereas with the addition of a silane coupling agent, this aggregation tendency diminishes. In sequence 2, the silica particles are most likely buried in the bulk and covered by LDPE. Hence, fewer dots are observed. As the silica loading increases, the aggregation tendency is expectedly more predominant.

In Figure 3, AFM images of blends containing 3 wt % nanosilica fillers, with and without a coupling agent, are shown. Comparing height and phase

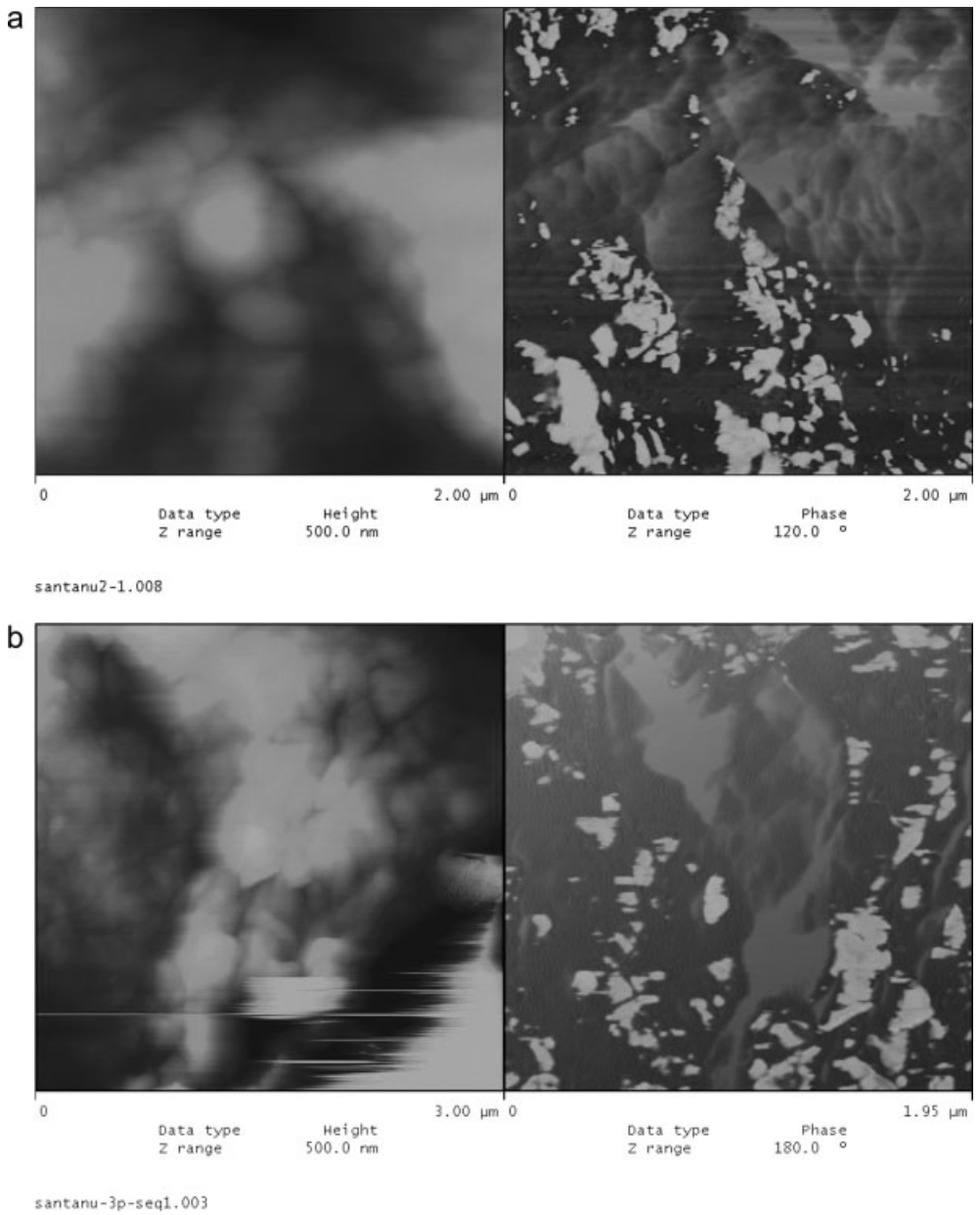

Figure 3 Height and phase AFM images of (a) ELS 6/4/3-3 and (b) ELS 6/4/3-3/Si-69. [Color figure can be viewed in the online issue, which is available at www.interscience.wiley.com.]

images, we find that darker domains correspond to the EVA portion of the blend and the lighter part represents the continuous LDPE matrix. Particles of various size scales (aggregate sizes) are distributed in the elastomeric matrix. The size scales span from the submicrometer range to the nanoscale range. Hence, the silica reinforcement achieved here is a composite of microscale and nanoscale reinforcements. Upon the addition of a coupling agent, however, the distribution turns out to be more uniform within the EVA matrix. This indicates a scope for further modifying the silica surface to achieve a greater degree of reinforcement. A detailed investigation of microscopic studies of these blend systems is in progress.

DSC

The DSC results are shown in Table II, and the DSC thermogram in Figure 4 exhibits a plot of the heat flow versus the temperature for various samples. Pure EVA shows a β transition at around −30°C. In the case of pure EVA, this β transition is generally considered the glass–rubber relaxation. The β transition is associated with the branch points containing the side group (vinyl acetate). The β peak becomes

TABLE II
DSC Results

Sample code	Third-cycle β relaxation (°C)	First cycle			
		T_1 (°C)	T_2 (°C)	Peak area (J/g)	T_m (°C)
E 100	−30	38	73	9.65	—
L 100	—	65	117	79.81	107
EL 6/4	−30	71	114	30.13	105
ELS 6/4/1.5	−31	74	113	28.86	105
ELS 6/4/3-1	−30	72	115	27.71	106
ELS 6/4/3-2	−30	72	112	26.33	106
ELS 6/4/3-3	−30	71	113	30.05	105
ELS 6/4/3-3/Si-69	−30	72	113	26.67	105
ELS 6/4/5	−30	70	113	30.01	105

E, EVA; L, LDPE; S, silica; T_1, temperature for onset of melting; T_2, temperature for completion of melting; T_m, melting temperature.

prominent if the concentration of the side groups exceeds a certain limit.[59] Furthermore, in EVA, a low-temperature endothermic peak around 41°C can also be observed. Thus, it is evident that the pristine EVA used in this study contains a very small number of crystalline features. On the other hand, pure LDPE exhibits one broad endothermic relaxation due to the crystalline melting (a peak around 107°C), which may also be associated with the α relaxation (representative of the segmental motion of the crystalline phase). The γ relaxation is associated with the crankshaft motion of the polymethylene groups of the main-chain backbone. The γ relaxation normally occurs in the range of −150 to −100°C (conventionally considered the glass transition of LDPE). However, in our study, the γ transition of pure LDPE has not been detected clearly. This may be due to interference from the crystalline zone. Upon the blending of EVA and LDPE, the characteristic transitions of the individual phases are not changed significantly. However, one additional endothermic peak appeared in a control blend sample, demonstrating a possibility of cocrystallization. When nanosilica particles were added to the blend, no significant change in the main melting peak corresponding to the LDPE phase was observed. However, in comparison with the control, the melting enthalpy of the filled matrix was reduced.

An important observation to note here is that the melting enthalpy remains more or less constant when 3 wt % silica is added in sequence 3. However, in the other two sequences, the probability of silica particles present in polyethylene is obviously greater. Hence, their effect on crystallinity is expected to be greater. Upon the use of a silane coupling agent, the area under the main melting endothermic peak diminishes significantly.

XRD

XRD patterns of various samples are shown in Figure 5. In all blends and in pure LDPE (not shown), there exist mainly two crystalline peaks in the diffraction pattern, one in the angular range (θ) of 12.3–12.5° and another between 13.6 and 13.8°. These peaks are well characterized in LDPE and correspond to specific crystallographic planes [110 and 200, respectively (Miller indices)].[58] On the other hand, EVA contributes only to the amorphous portion in the blend.

P, r, and d (calculated with respect to the peak in the angular range of 12.3–12.5°) and κ_c of the samples are shown in Table III.

No significant changes in r or d have been observed in the blend systems studied here. When silica particles are introduced into the polymer

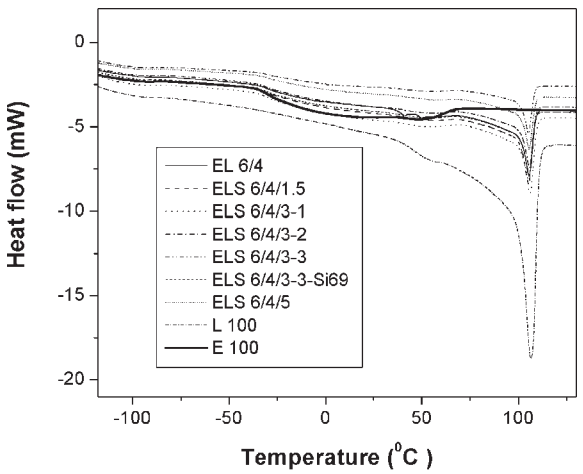

Figure 4 DSC thermogram of 60 : 40 blends of EVA and LDPE with different loadings of nanosilica particles.

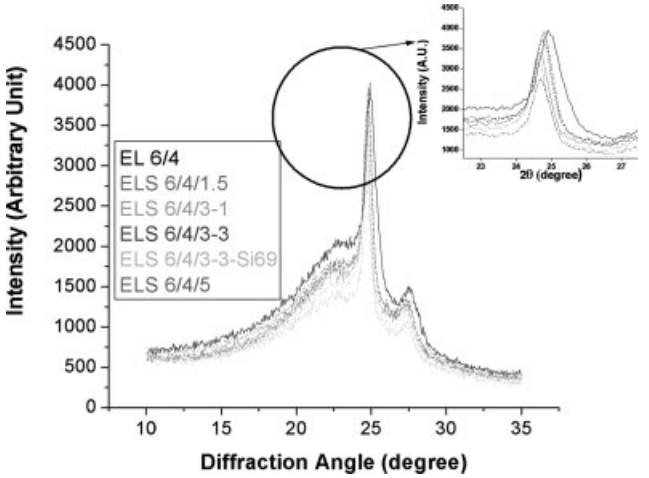

Figure 5 XRD patterns of 60 : 40 blends (intensity vs 2θ) of EVA and LDPE with various loadings of nanosilica. [Color figure can be viewed in the online issue, which is available at www.interscience.wiley.com.]

matrix, κ_c decreases because of the destruction of the crystallites in comparison with the unfilled one. This is also confirmed by a peak area analysis of the DSC measurements, as demonstrated earlier. Another important observation can be noted here: although κ_c decreases in the filled matrix in comparison with the control, P increases.

The literature reveals that silica particles can act as nucleating agents in the polyolefin matrix and consequently can facilitate crystallization.[44] However, when the particles are too small (15 nm), they may locate themselves in the interlamellar spaces, leaving little room for additional crystallization.[45] Therefore, the presence of these particles may inhibit the crystallization of the whole polymer matrix, but because of their nucleating tendency, P may increase.

Although, in comparison with DSC analysis, quasicrystalline patterns are difficult to capture in XRD in general, in our case, the trend in both analyses remains essentially constant.

Mechanical properties

Tensile tests were performed to investigate the mechanical properties of samples with various compositions and methods of preparation. The average mechanical properties are given in Table IV. Within sequence 3, the tensile strength initially increases with the silica loading, reaches its maximum value at a loading of 3 wt %, and decreases with a further increase in the silica loading. On the contrary, both high- and low-strain moduli decrease with an increase in the filler loading. The elongation at break is improved only for samples with a 3 wt % silica loading.

At a constant loading of 3 wt % silica, the maximum tensile strength is observed in sequence 3. In sequence 2, the tensile strength registers its minimum value, which is comparable to that of the control sample (without a silica loading). Sequence 1 remains between sequences 2 and 3. The trend of the low-strain modulus with the variation of the sequence at a constant loading remains similar to that of the tensile strength. The elongation at break of sequences 1 and 2 is comparable to that of the control sample, but sequence 3 registers a slightly higher value.

However, the addition of a coupling agent in sequence 3 drastically improves all the mechanical properties in comparison with the rest of the samples. The tensile strength is improved by 41.0%, the 100% modulus is improved by 6.5%, the 200% modulus is improved by 10%, the 300% modulus is improved by 30%, and the low-strain (3% elongation) modulus is improved by 14%. The elongation at break is also somewhat increased.

However, in all cases, the tension set is improved in comparison with the control. The minimum set is observed in samples having a higher filler loading within sequence 3. In a sample prepared with sequence 3, the set is further improved upon the addition of a coupling agent. In sequence 2, the set is unexpectedly high because of the dramatic change in the morphology in comparison with the other samples, as evidenced by the morphological analysis.

The initial increase in the tensile strength up to a 3 wt % loading of silica is possibly due to the increase in the interfacial interaction, which eliminates the possibility of the formation and propagation of cracks at the interface during stretching. Also, at a 3 wt % loading, the unmodified silica particles are optimally dispersed in the elastomeric phases in comparison with other loadings, providing a better reinforcement effect. On the other hand, because the surfaces of the silica particles are not modified, filler–polymer interactions are not manifested in increases in the elongation percentage and

TABLE III
XRD Results for Various Samples

	X-ray studies			
Sample code	κ_c (%)	P (Å)	r (Å)	d (Å)
EL 6/4	15.2	120	4.46	3.6
ELS 6/4/1.5	12.9	156	4.50	3.6
ELS 6/4/3-1	13.2	153	4.52	3.6
ELS 6/4/3-3	14.1	153	4.49	3.6
ELS 6/4/3-3/Si-69	13.4	152	4.51	3.6
ELS 6/4/5	14.2	160	4.49	3.6

E, EVA; L, LDPE; S, silica.

TABLE IV
Mechanical Properties of the Films Made from Various Blends

Sample code	Tensile strength (MPa)	Elongation at break (%)	Modulus (MPa)				Set (%)
			100%	200%	300%	3%	
EL 6/4	3.4	480	2.63	2.90	3.13	6.4	16.8
ELS 6/4/1.5	3.8	478	2.62	2.93	3.26	5.9	15.0
ELS 6/4/3-1	3.9	479	2.48	2.87	3.23	6.1	14.0
ELS 6/4/3-2	3.4	465	2.24	2.62	2.97	5.3	26.0
ELS 6/4/3-3	4.0	520	2.56	2.85	3.13	6.2	13.0
ELS 6/4/3-3/Si-69	4.8	490	2.80	3.20	4.10	7.3	12.5
ELS 6/4/5	3.5	450	2.28	2.6	2.91	5.6	12.0

E, EVA; L, LDPE; S, silica.

modulus. At higher loadings, the tensile strength and modulus are not affected greatly. This can be ascribed to the aggregation of fillers leading to the occurrence of low-energy deformation modes, such as aggregate breakage, aggregate–polymer interface breakage, and breakage through the defect sites. Thus, it dilutes the reinforcement effect.

In comparison with the other sequences, in sequence 3, property enhancement is maximum. Because in this particular sequence silica is initially blended with the more polar EVA phase, the silica distribution is more uniform here, leading to the strengthening of the weaker phase of the blend system (as observed in the morphological analysis). However, in sequence 2, because silica is premixed with the relatively nonpolar LDPE matrix, the chances of aggregate formation are obviously greater. Moreover, it may adversely affect the crystallization behavior of LDPE as such (as evidenced by XRD and DSC analysis). In sequence 1, on the other hand, an equivalent probability of the distribution of silica particles in both the LDPE and EVA phases exists. This explains the differences in the mechanical properties with respect to the variation of the sequence of mixing.

A dramatic improvement in the tensile strength and modulus can be observed upon the addition of a silane coupling agent. The elongation at break is also slightly improved in comparison with that of the control sample. The inclusion of a coupling agent such as Si-69 increases the interaction between the weak EVA network and silica, reduces the filler–filler interaction by breaking the agglomerated structure, and increases the interaction between the particles and polymer (as shown in AFM studies in an earlier section). Also, in the presence of a coupling agent, interfacial adhesion between EVA and LDPE is possibly improved to a certain extent (as indicated by SEM earlier).

The improvement of the set properties can be explained on the basis of an improvement of the recovery of the polar EVA matrix in the presence of silica fillers.

DMA

DMA is used as a sensitive method for identifying interfacial interactions in composites. Generally, strong interactions between the nanoparticles and the matrix polymer can restrict the movement of polymer segments near the particles, and this would be reflected in changes in the modulus–temperature response of the matrix. A dynamic mechanical thermal analysis of various samples was performed. Plots of the storage modulus versus the temperature and tan δ versus the temperature for various samples are shown in Figures 6 and 7, respectively.

Control LDPE exhibits three major relaxations, which are termed the α, β, and γ relaxations. The α relaxation occurs in the temperature range of 30–100°C and is representative of the crystalline phase. The β relaxation occurs in the range of −30 to 10°C and is attributed to the amorphous phase. The γ relaxation is associated with the crankshaft motion of the polymethylene groups of the main-chain backbone. The γ relaxation normally occurs in the range

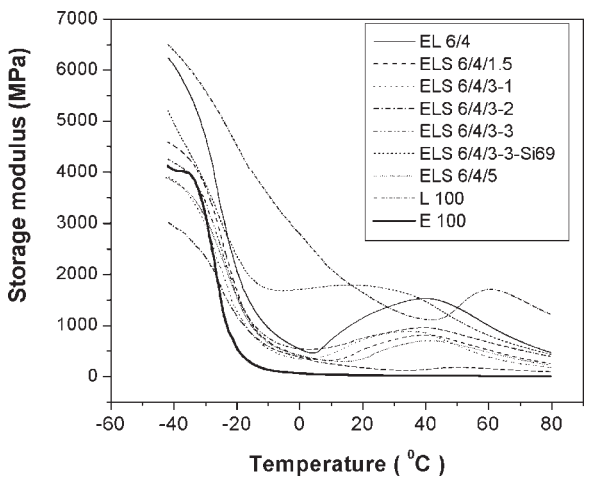

Figure 6 Variation of the storage modulus with the temperature for 60 : 40 EVA–LDPE blends with various loadings of nanosilica and with variations in the sequence.

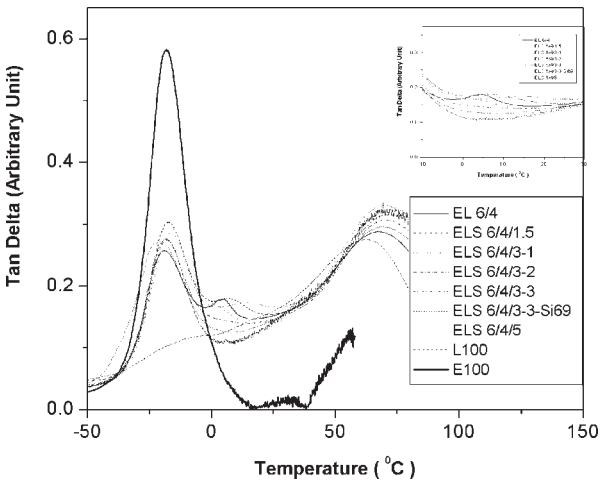

Figure 7 Variation of tan δ with the temperature for 60 : 40 EVA–LDPE blends with different loadings of nanosilica and with variations in the sequence.

of −150 to −100°C (conventionally considered the glass transition of LDPE) and is not detectable here. The mechanism of the α transition is believed to be due to the vibration–rotational motion of the polymer chain within the crystalline zone.[60] Additionally, one broad peak at 62°C can be observed for LDPE. The β relaxation is associated with the branch points containing the side group. The β relaxation becomes prominent if the concentration of the side groups exceeds a certain limit. However, we could not locate a prominent β relaxation for LDPE in our study. Pristine EVA, on the other hand, exhibits two main relaxations at −19 and 57°C. The relaxation around −19°C is assigned to the β relaxation (considered to be the glass transition of EVA), and a weaker relaxation at 57°C is due to the α relaxation.[61]

The relaxation at 57°C corresponding to EVA and the LDPE relaxation at 62°C are merged and shifted toward a higher temperature for the control blend. This trend also persists in the blends containing silica filler. The polymer–nanosilica interaction is evidenced by the shift of the β-relaxation peak (corresponding to the maximum tan δ) of EVA toward a higher temperature. The tan δ plot of the control blend registers three peaks at −19, 4, and 67°C (Fig. 7). We presume that the relaxation at 4°C is due to the interface between the EVA and LDPE domains. When 1.5 wt % pristine silica is added, three peaks appear at −16, 7, and 71°C; that is, all transitions are shifted to higher temperatures. With the 3 wt % sample, two peaks can be clearly observed at −18 and 70°C, respectively. However, the relaxation at an intermediate temperature is not prominent there. Interestingly, the value of tan δ corresponding to β relaxation pursues the following order: 1.5 wt % > 5 wt % > 3 wt % > control. This possibly indicates that with a 3 wt % silica loading, an optimum dispersion of silica in the EVA phase is obtained. This is also indicated in the earlier sections. Also, in the 5 wt % silica loaded samples, two transitions at −17 and 71°C along with a feeble relaxation at 16°C can be observed. An increase in the storage modulus with the temperature up to 40°C is indicative of cocrystallization of all the blends. This is, however, markedly absent in pristine polyethylene. The modulus essentially starts falling off afterwards because of the onset of the α relaxation.

However, in the other two sequences, a relaxation at an intermediate temperature is not observed. Thus, the silica dispersion and distribution have an important role in modifying the gross relaxation behavior of the blends. In sequence 1, changes in the dynamic storage modulus/temperature behavior are similar to those in sequence 3. However, the maximum tan δ value of the former is greater than that of later. Indeed, in this case, the value of tan δ (maximum) is highest among all the blends studied here. Above 40°C, sequence 1 registers a faster fall of the modulus with the temperature. In sequence 2, the β relaxation is similar to that of the control blend, but at higher temperatures, it does not record cocrystallization (similar to pristine LDPE). The dynamic modulus of this particular blend at the ambient temperature is lowest and very close to that of the weaker EVA phase. Thus, it is quite obvious that in sequence 2, an altogether different morphology is developed, which has been demonstrated in earlier sections.

When 3 wt % silica along with Si-69 is added, the β transition is shifted to a lower temperature, and the area under the tan δ/temperature curve becomes maximum; this indicates a broader relaxation process. The peak maximum (maximum tan δ) also shifts to a lower temperature. This is indicative of compatibilization of the silica filler in the EVA matrix in the presence of Si-69. Also, in this case, a prominent rubbery plateau can be observed for the first time. The average dynamic modulus at the ambient temperature is increased up to 35% in comparison with the control samples. Another important point to note at this stage is that the rate of decrease in the modulus after 40°C is much slower here in comparison with the other filled samples, and the higher temperature modulus value matches well that of the control sample. Therefore, the increase in the mechanical and dynamic mechanical properties in this composite mainly originates from the reinforcement of the EVA phase and interface, not from the generation of additional crystallite features (indeed, κ_c is reduced, as shown by XRD and DSC studies).

CONCLUSIONS

Nanoscale pristine silica, when dispersed in LDPE–EVA-based TPE systems, alters the microscale morphology of the blend systems as well as their crystalline morphology. This is a strong function of the sequence and extent of nanosilica addition. In sequences 1 and 3, comparatively superior mechanical and dynamic mechanical properties result in comparison with those of sequence 2. A 3 wt % silica concentration was found to be the optimum loading in sequence 3. Silica associates more in the EVA phase than with the LDPE matrix even in sequence 1. The addition of a silane coupling agent (Si-69) to the formulation of silica-filled polymer blends leads to significant increases in the tensile strength, modulus, extensibility, and dynamic properties of the blends. An AFM study has revealed that the distribution of silica fillers becomes more uniform in the presence of Si-69. However, κ_c of the blends is reduced because of the addition of the coupling agent. Therefore, a greater degree of reinforcement can be achieved by facilitation of reinforcement due to crystallization along with a finer nanoscale dispersion of silica to reinforce weaker elastomeric EVA domains.

References

1. Lee, M. W.; Hu, X.; Yue, C. Y.; Li, L.; Tam, K. C. Compos Sci Technol 2003, 63, 339.
2. Lee, M. W.; Hu, X.; Yue, L. L.; Tam, K. C.; Nakayama, K. J Appl Polym Sci 2002, 86, 2070.
3. Joshi, M.; Maiti, S.; Mishra, A. Polymer 1994, 35, 3679.
4. Gnatowski, A.; Koszkul, J. J Mater Proc Technol 2005, 52, 162.
5. Xu, X. B.; Li, Z. M.; Yang, M. B.; Jiang, S.; Huang, R. Carbon 2005, 43, 1479.
6. Shumsky, V. F.; Lipatov, Y. U. S.; Kulichikhin, V. G.; Getmanchuk, I. P. Rheol Acta 1993, 32, 352.
7. Denac, M.; Musil, V.; Mit, I. J Polym Sci Part B: Polym Phys 2004, 42, 1255.
8. Tjong, S. C.; Meng, Y. Z. Polymer 1999, 40, 1109.
9. Khatua, B. B.; Lee, D. J.; Kim, J. K. Macromolecules 2004, 37, 2454.
10. Lee, K. M.; Han, C. D. Macromolecules 2003, 36, 7165.
11. Gao, X.; Qu, C.; Zhang, Q.; Peng, Y.; Fu, Q. Macromol Mater Eng 2004, 289, 41.
12. Ginzburg, V. V.; Qiu, F.; Paniconi, M.; Peng, G.; Jasnow, D.; Balazs, A. C. Phys Rev Lett 1999, 82, 4026.
13. Ginzburg, V. V.; Peng, G.; Qiu, F.; Jasnow, D.; Balazs, A. C. Phys Rev E 1999, 60, 4352.
14. Balazs, A. C.; Ginzburg, V. V.; Qiu, F.; Peng, G.; Jasnow, D. J Phys Chem B 2000, 104, 3411.
15. Zhu, Y. J.; Ma, Y. Q. Phys Rev E 2003, 67, 041503.
16. Laradji, M.; MacNevin, G. J Chem Phys 2003, 119, 2275.
17. Laradji, M. J Chem Phys 2004, 120, 9330.
18. Tanaka, H.; Lovinger, A. J.; Davis, D. D. Phys Rev Lett 1994, 72, 2581.
19. Lipatov, Y. S. Prog Polym Sci 2002, 27, 1721.
20. Lipatov, Y. S.; Nesterov, A. E.; Ignatova, T. D.; Nesterov, D. A. Polymer 2002, 43, 875.
21. Nesterov, A. E.; Lipatov, Y. S. Polymer 1999, 40, 1347.
22. Wu, G.; Asai, S.; Sumita, M.; Yui, H. Macromolecules 2002, 35, 945.
23. Sumita, M.; Sakata, K.; Hayakawa, Y. Colloid Polym Sci 1992, 270, 134.
24. Kaneko, H.; Inoue, K.; Tominaga, Y.; Asai, S.; Sumita, M. Mater Lett 2002, 52, 96.
25. Huh, J.; Ginzburg, V. V.; Balazs, A. C. Macromolecules 2000, 33, 8085.
26. Thompson, R. B.; Ginzburg, V. V.; Matsen, M. W.; Balazs, A. C. Science 2001, 292, 2469.
27. Thompson, R. B.; Ginzburg, V. V.; Matsen, M. W.; Balazs, A. C. Macromolecules 2002, 35, 1060.
28. Shou, Z.; Buxton, G. A.; Balazs, A. C. Compos Interfaces 2003, 10, 343.
29. Lee, J. Y.; Balazs, A. C.; Thompson, R. B.; Hill, R. M. Macromolecules 2004, 37, 3536.
30. Lee, J. Y.; Thompson, R. B.; Jasnow, D.; Balazs, A. C. Macromolecules 2002, 35, 4855.
31. Wang, Y. T.; Chang, T. C.; Hong, Y. S.; Chen, H. B. Thermochim Acta 2003, 397, 219.
32. Wu, R.; Xie, C. S.; Xia, H.; Hu, J. H.; Wang, A. H. J Cryst Growth 2000, 217, 274.
33. Li, R. X.; Yabe, S.; Yamashita, M.; Momose, S.; Yoshida, S.; Yin, S.; Sato, T. Mater Chem Phys 2002, 75, 39.
34. Xiong, M. N.; Wu, L. M.; Zhou, S. X.; You, B. Polym Int 2002, 51, 693.
35. Zhou, S. X.; Wu, L. M.; Sun, J.; Shen, W. D. Prog Org Coat 2002, 45, 33.
36. Zhou, S. X.; Wu, L. M.; You, B. J Appl Polym Sci 2003, 88, 189.
37. Filipe, S.; Cidade, M. T.; Wilhelm, M.; Maia, J. M. Polymer 2004, 45, 2367.
38. Lee, J. K.; Han, C. D. Polymer 2000, 41, 1799.
39. Farasoglou, P.; Kontou, E.; Spanthis, G.; Gomez-Ribelles, J. L.; Gallego, F. G. Polym Compos 2000, 21, 84.
40. Gopakumar, T. G.; Ponarathnam, S.; Rajan, C. R.; Fradet, A. Polymer 1998, 39, 2221.
41. Silverstein, M. S.; Hiltner, A.; Baer, E. J Appl Polym Sci 1991, 43, 157.
42. Shuster, R. H. Int Polym Sci Technol 1996, 23, 11.
43. Lu, H.; Xu, X.; Li, X.; Zhang, Z. Bull Mater Sci 2006, 29, 485.
44. Li, H.; Zhan, R.; Li, Y. J Reinforced Plast Compos 2006, 25, 1001.
45. Luyt, A. S.; Molefi, J. A.; Krump, H. Polym Degrad Stab 2006, 91, 1629.
46. Wu, Z.; Zhou, C.; Oi, C.; Zhang, H. J Appl Polym Sci 2002, 83, 2403.
47. Goettler, L. A.; Lee, K. Y.; Thakkar, H. Polym Rev 2007, 47, 291.
48. Naderi, G.; Lafleur, P. G.; Dubois, C. Polym Eng Sci 2007, 47, 207.
49. Pukanszky, B. Composites 1990, 21, 255.
50. Bazgir, S.; Katbab, A. A.; Nazockdast, H. J Appl Polym Sci 2004, 92, 2000.
51. Karim, A.; Liu, D. W.; Douglas, J. F.; Nakatani, A. I.; Amis, E. J. Polymer 2000, 41, 8455.
52. Scott, C. J Reinforced Plast Compos 1991, 10, 463.
53. Mukhopadhyay, P.; Das, C. K.; Sawarkar, S. K. Int J Polym Mater 1987, 12, 65.
54. Tchoudakov, R.; Breuer, O.; Narkis, M. Polym Eng Sci 1996, 36, 1336.
55. Torres, R. A.; Arellano-Ceja, J.; Hernández-Hernández, M. E.; González-Núñez, R. Polym Bull 2007, 59, 251.
56. Dasari, A.; Yu, Z.-Z.; Mai, Y.-W. Polymer 2005, 46, 5986.
57. Dasari, A.; Yu, Z.-Z.; Yang, M.; Zhang, Q.-X.; Xie, X.-L.; Mai, Y.-W. Compos Sci Technol 2006, 66, 3097.
58. Alexander, L. E. X-Ray Diffraction Methods in Polymer Science; Wiley-Interscience: New York, 1969; p 335.
59. Oakes, W. G.; Robinson, D. W. J Polym Sci 1954, 14, 505.
60. Lee, H.; Cho, K.; Ahn, T.-K.; Choe, S.; Kim, I.-J.; Park, I.; Lee, H. B. J Polym Sci Part B: Polym Phys 1997, 35, 1633.
61. Arsac, A.; Carrot, C.; Guillet, J. J Appl Polym Sci 1999, 74, 2625.